Potential of Interactive Multiobjective Optimization in Supporting the Design of a Groundwater Biodenitrification Process

Giulia Saccani [a], Jussi Hakanen [b], Karthik Sindhya [b], Vesa Ojalehto [b], Markus Hartikainen [b], Manuela Antonelli [a]*, Kaisa Miettinen [b] **

[a] Politecnico di Milano, Department of Civil and Environmental Engineering (DICA), Piazza Leonardo da Vinci 32, 20133 Milan, Italy. e-mails: giulia.saccani@polimi.it ; manuela.antonelli@polimi.it

[b] University of Jyvaskyla, Faculty of Information Technology, P.O. Box 35 (Agora), FI-40014 University of Jyvaskyla, Finland. e-mail: jussi.hakanen@jyu.fi ; karthik.sindhya@jyu.fi ; vesa.ojalehto@jyu.fi ; markus.hartikainen@jyu.fi ; kaisa.miettinen@jyu.fi

* Corresponding author: Manuela Antonelli Tel.: +39 02 2399 6407; fax: +39 02 2399 6499. E-mail address: manuela.antonelli@polimi.it

** Co-Corresponding Author: Kaisa Miettinen Tel. +358 503 732 247. E-mail address: kaisa.miettinen@jyu.fi

Contents of this file

SUPPLEMENTARY MATERIAL

Text S1. Conceptual representation of the design optimization problem

The iterative multiobjective design optimization problem is sketched in the flowchart reported in Figure S1.

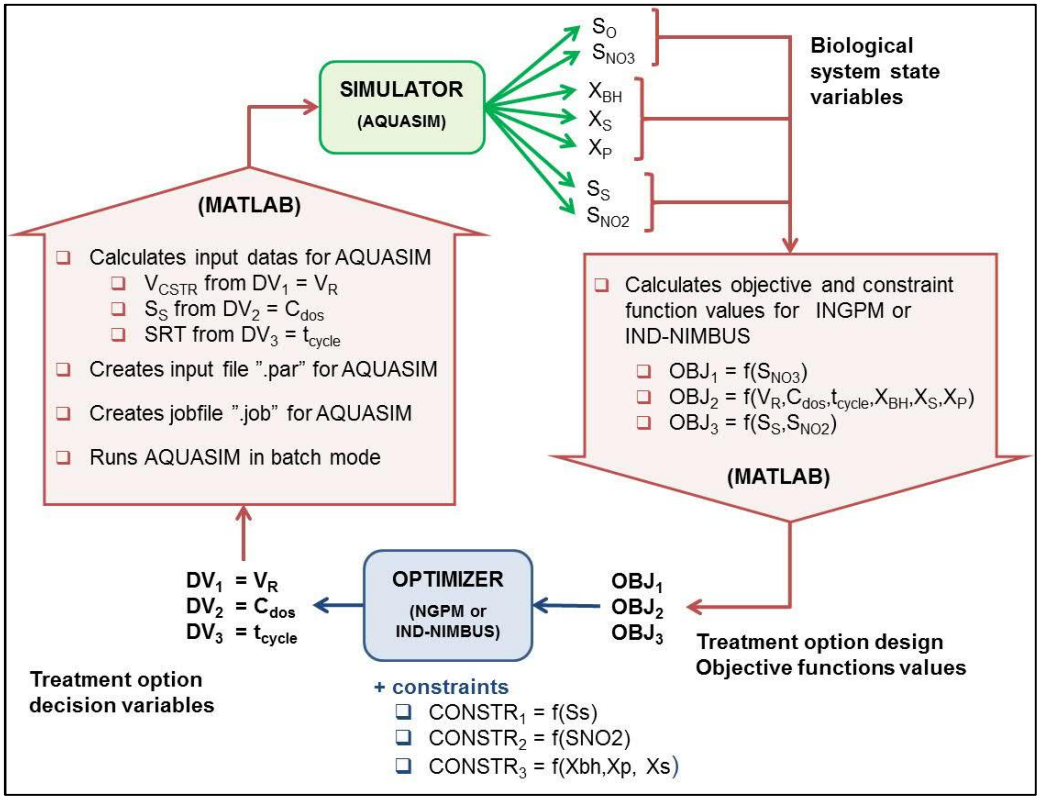

Figure S1. Flowchart representing the design optimization problem constituting units

Text S2. Hydraulic characterization of the biofilter

The hydraulic characterization has been performed by an impulsive tracer test, obtaining the Residence Time Distribution (RTD) and calculating the average hydraulic retention time (HRT). Four campaigns were performed. In the first one, before the biofilter colonization, NaCl was used (16.5 g NaCl), monitoring the conductivity of the water at the filter outlet. In the others campaigns, LiCl was used sampling effluent water at intervals of time defined by the results of the NaCl tracer tests. LiCl has been used as tracer as it doesn't present any toxicity, inhibition or accumulation effect on biomass (Séguret e Racault, 1998; Olivet et al., 2005). The first campaign with LiCl (4.2 mg LiCl) was carried out before biofiler colonization, the second and third campaigns were carried out immediately after the biofilter start-up phase (1.1 mg LiCl) and at the end of the process evaluation phase (1.0 mg LiCl). All tracer tests were performed at continuous flow rate of 0.6 m3/h.

Text S3. Biofilter simulation model

The biofilter has been hydraulically modelled as eight CSTRs in series, as in Figure S.2.

Attached biomass biofilter is reported to be modelled through different kinds of biofilm models (Boltz et al., 2010; Huang et al., 1998; Morgenroth et al., 2000). However, these models have become more and more

complex (Morgenroth et al., 2000) and, when the main modelling purpose is the prediction of biofilter removal efficiency, simpler models can be applied (Lazarova et al., 1994, 1992; Vrtovšek and Roš, 2006) considering only the pollutant removal rate (i.e. denitrification rate) without any simulation of biomass growth and decay processes. A good trade-off among model simplicity and predictability of both dissolved and particulate matter concentrations is represented by variations of the Activated Sludge Models (ASM) that are reported to be applied for attached biomass systems as Moving Bed Bioreactors (Plattes et al., 2007, 2006) and submerged bioreactors (Huang et al., 1998; Ordaz et al., 2012). However, none of the ASM models (not even ASM2) is able to predict concentrations of nitrite produced during nitrate reduction, since it considers denitrification as a one step process (i.e., nitrate reduction to nitrogen biogas). Anyway, in drinking water treatment, nitrite accumulation cannot be neglected as it is a known carcinogen whose concentration is subjected to a stringent regulation limit. Therefore, more properly, a 2-step denitrification kinetic should to be considered.

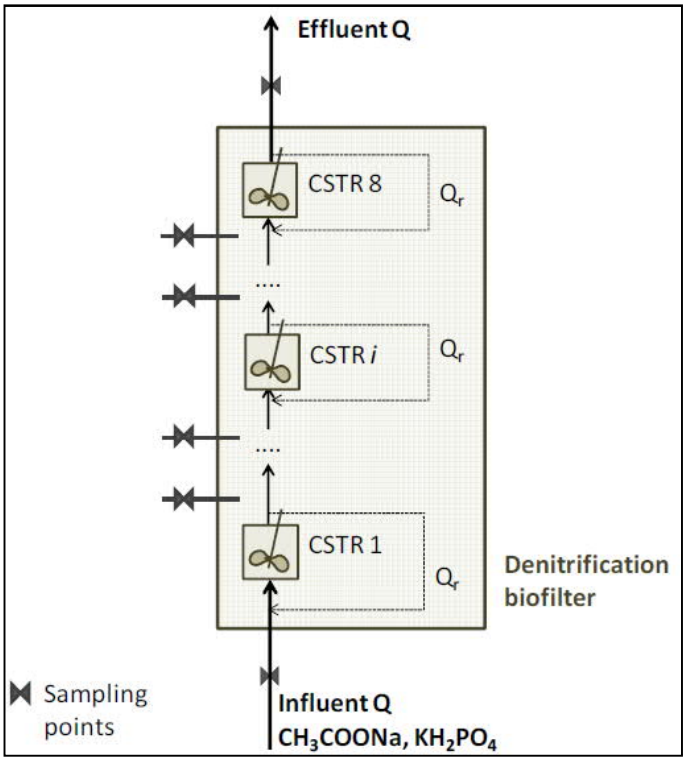

Figure S2. Hydraulic modelling of the pilot biofilter through 8 CSTRs in series

Table S1. Biological and physical processes assumed to occur in the biofilter following ASM1 [Henze et al., 2000]

Process name	S_S	S_O	S_{NO_2}	S_{NO_3}	X_{BH}	X_S	X_P	RATE
Aerobic Growth	$-\frac{1}{Y_H}$	$-\frac{1-Y_H}{Y_H}$		$-i_{XB}$	1			r_1
Anoxic Growth NO_3	$-\frac{1}{Y_H}$		$+\frac{1-Y_H}{1{,}14 \cdot Y_H}$	$-\frac{1-Y_H}{1{,}14 \cdot Y_H}$ $-i_{XB}$	1			r_2

Anoxic Growth NO_2	$-\frac{1}{Y_H}$		$-\frac{1-Y_H}{1{,}71 \cdot Y_H} - i_{XB}$		1			r_3
Decay					-1	$1-f_p$	f_p	r_4
Hydrolysis	1					-1		r_5

65

66 **Table S2.** Process rates in $mg_{COD}/L \cdot d$ taken from ASM1 by Henze et al. [2000] [1], 2-step denitrification models
67 by Magrì and Flotats [2008] [2], Kornaros and Lyberatos [1998] [3].

Name	Process	Expression
$\mathbf{r_1}$ [1]	Aerobic Growth	$\hat{\mu}_H \cdot \left(\frac{S_S}{S_S + k_s}\right) \cdot \left(\frac{S_O}{S_O + k_{O,H}}\right) \cdot X_{BH} \cdot \vartheta^{T-20}$
$\mathbf{r_2}$ [2]	Anoxic growth on nitrate	$\eta_{g1} \cdot \hat{\mu}_H \cdot \left(\frac{S_S}{S_S + k_S}\right) \cdot \left(\frac{S_{NO3}}{S_{NO3} + k_{NO3}}\right) \cdot \left(\frac{k_O}{k_O + S_O}\right) \cdot X_{BH} \cdot \vartheta^{T-20}$
$\mathbf{r_3}$ [3]	Anoxic growth on nitrite	$\eta_{g2} \cdot \hat{\mu}_H \cdot \left(\frac{S_S}{S_S + k_S}\right) \cdot \left(\frac{S_{NO2}}{S_{NO2} + k_{NO2}}\right) \cdot \left(\frac{k_O}{k_O + S_O}\right) \cdot \left(\frac{k_{I,NO3}}{k_{I,NO3} + S_{NO3}}\right) \cdot X_{BH} \cdot \vartheta^{T-20}$
$\mathbf{r_4}$ [1]	Biomass decay	$b_H \cdot X_{BH} \cdot \vartheta^{T-20}$
$\mathbf{r_5}$ [1]	Hydrolysis of entrapped organics	$k_h \cdot \frac{X_S}{K_X \cdot X_{BH} + X_S} \cdot \left[\left(\frac{S_O}{S_O + k_{O,H}}\right) + \eta_h \cdot \left(\frac{k_{O,H}}{S_O + k_{O,H}}\right) \cdot \left(\frac{S_{NO3} + S_{NO2}}{S_{NO3} + S_{NO2} + k_{NO}}\right)\right] \cdot X_{BH}$

68

69 **Table S3.** Model parameters values taken from: ASM1 by Henze et al. (Henze et al., 2000) [1], 2-step
70 denitrification models by Magrì and Flotats (Magrí and Flotats, 2008) [2], Kornaros and Lyberatos (Kornaros
71 and Lyberatos, 1998) [3] and bioenergetic evaluations by Henze et al. (Henze et al., 2008) [4].

Parameter	Value	Unit	Meaning
$\mathbf{X_{BH,0}}$	0.01	mg_{COD}/L	Initial concentration of heterotrophic active biomass
$\mathbf{X_{P,in}}$	0.01	mg_{COD}/L	Influent concentration of non-biodegradable particulate matter
$\mathbf{X_{S,in}}$	0.01	mg_{COD}/L	Influent concentration of slowly-biodegradable substrate
$\hat{\mu}_H$	4.16[2]	1/d	Maximum specific growth rate for heterotrophic biomass
$\mathbf{b_H}$	0.62[1]	1/d	Decay rate for heterotrophic biomass
$\mathbf{k_h}$	3.0[1]	1/d	Maximum specific hydrolysis rate
$\boldsymbol{\theta}$	1.03[1]	-	Correction factor for temperature effect on biomass growth and decay rates
$\boldsymbol{\eta_{g1}}$	0.23[2]	-	Correction factor for μ_h for anoxic growth on nitrate-nitrogen
$\boldsymbol{\eta_{g2}}$	0.592[3]	-	Correction factor for μ_h for anoxic growth on nitrite-nitrogen
$\boldsymbol{\eta_h}$	0.4[1]	-	Correction factor for hydrolysis under anoxic conditions
$\mathbf{k_s}$	4[2]	mg_{COD}/L	Half-saturation constant for organic substrate

$k_{O,H}$	0.2[1]	mg_{COD}/L	Half-saturation constant for oxygen
k_{NO3}	0.5[2]	mg_N/L	Half-saturation constant for nitrate nitrogen
k_{NO2}	0.28[3]	mg_N/L	Half-saturation constant for nitrite nitrogen
k_X	0.03[1]	-	Half-saturation constant for slowly biodegradable substrate
$k_{I,NO3}$	8.75[3]	mg_N/L	Nitrate inhibition constant
Y_h	0.46[4]	mg_{COD}/mg_{COD}	Heterotrophic biomass yield, considering NO_3-N uptake for protein synthesis
f_p	0.08[1]	-	Fraction of biomass leading to particulate products
i_{XB}	0.086[1]	mg_N/mg_{COD}	Mass of nitrogen per mass of COD in biomass

Text S4. Optimization problem formulation

The definition of design variables, objective functions and constraints for the multiobjective design optimization problem has been driven by considerations based on practical experience and literature data.

For **design variables**, lower and upper bounds had to be indicated. Bounds for reactor volume (V_r, expressed in L) have been defined by assuming acceptable values for denitrification contact time (Empty Bed Contact Time, EBCT). Richard (Richard, 1989) reports an EBCT of 23-38 min and 22-43 min for two different full scale groundwater denitrification biofilters with expanded clay as biomass carrier. These values are in agreement with recommendations reported by Metcalf and Eddy (Tchobanoglous et al., 2014), who suggest EBCT values in the range of 20-30 min for submerged denitrification reactors, and by Pujol et al. (Pujol et al., 1994), who suggest 15-60 min as a possible EBCT range. Nurizzo and Mezzanotte (Nurizzo and Mezzanotte, 1992) report EBCTs in the range of 8-36 min for groundwater denitrification in a biofilter using sand as biomass support media of granules size comparable to expanded clay. EBCT was then set to vary within the range 5-120 min, leading to a reactor volume ranging between 50-1200 L.

As for the external carbon source dosage (C_{dos}, expressed in mg_{COD}/L), the lower bound corresponds to no carbon dosage (0 mg_{COD}/L) while the upper bound ($C_{dos,ub}$) was chosen in order not to set a practical limit to this variable. A value of 200 mg_{COD}/L was chosen, corresponding to a dosage four times higher than the stoichiometric requirements (see equations eq. S1 - S2), calculated considering influent electron acceptor concentrations reported in Table 1, stoichiometric ratios reported in Section 2.1 and 2.667 g_{COD}/g_C for sodium acetate dosage. This excess value is a reasonable upper bound: it should not imply any inhibition of denitrifying biomass when acetic acid is adopted as carbon source, as reported by Her and Huang (Her and Huang, 1995), who reached a 1600% carbon dosage excess. Furthermore, considering that Tang et al. (Tang et al., 2011) observed 19 mg_{COD}/L in the effluent just with a 25% excess of carbon dosage (as CH_3COONa), unacceptable carbon concentrations in the effluent should be limiting the optimal values of this design variable before reaching its upper bound, as desired.

$$C_{dos,ub} = \alpha \cdot \left[\left({}^{C}/_{DO} \right) \cdot DO_{in} + \left({}^{C}/_{NO_3 - N} \right) \cdot (NO_3 - N)_{in} + \left({}^{C}/_{NO_2 - N} \right) \cdot (NO_2 - N)_{in} \right] \cdot 2.667 \frac{mg_{COD}}{mg_C} \quad \text{(S1)}$$

$$C_{dos,ub} = 4 \cdot \left[0.70 \frac{g_C}{g_{DO}} \cdot 6.2 \frac{mg_{DO}}{L} + 1.69 \frac{g_C}{g_{NO_3-N}} \cdot 8.9 \frac{mg_{NO_3-N}}{L} + 1.27 \frac{g_C}{g_{NO_2-N}} \cdot 0.014 \frac{mg_{NO_2-N}}{L} \right] \cdot 2.667 \frac{mg_{COD}}{mg_C} \cong 200 \frac{mg_{COD}}{L} \quad \text{(S2)}$$

Finally, for Sludge Retention Time (SRT, expressed in days) lower and upper bounds were set, respectively, at 1 d and 100 d considering that MetCalf and Eddy (Tchobanoglous et al., 2014) report 20-40 d as typical SRT range for denitrifying submerged biofilters.

As for **objective functions**, the first and the third objectives were both expressed in terms of water measurable characteristics, as expressed by eq. S3 and eq. S4.

$$OBJ_1 = NO_3 - N_{out} \left[{}^{mg_N}/_{L} \right] = S_{NO3} \quad \text{(S3)}$$

$$OBJ_3 = COD_{out} \left[{}^{mg_{COD}}/_{L} \right] = S_S + S_{NO2} \cdot 1.71 \frac{mg_{COD}}{mg_N} \quad \text{(S4)}$$

On the other hand, the second objective function, representing investment and management costs, was defined based on data from practical experience and values refer to Italian prices and conditions. Considered costs were the ones significantly varying as a function of design variable variation:

- Reactor volume considerably affects investments costs ($Cost_{invest}$) in terms of cost of biofilter building works (160-200 €/m^3) and filling material requirements (500-630 €/m^3), as expressed by equation eq. S5:

$$Cost_{invest}[€] = (0.2 + 0.6) \frac{€}{L} \cdot V_R \quad \text{(S5)}$$

- Carbon dosage considerably affects management costs ($Cost_{reag}$) in terms of reagent supply (850 €/t of CH_3COOH as 15% solution). The reagent supply costs have been calculated by equation eq. S6, considering 2.667 g_{COD}/g_C in case of acetic acid dosage.

$$Cost_{reag} \left[{}^{€}/_{yr} \right] = \frac{C_{dos} \cdot 14400 \frac{L}{d}}{2.667 \, {}^{g_{COD}}/_{g_C}} \cdot \frac{60 \, {}^{g_{AC}}/_{mol}}{24 \, {}^{g_C}/_{mol}} \cdot \frac{1}{0.15} \cdot \frac{365 \frac{d}{yr}}{10^6 \frac{mg}{kg}} \cdot 0.85 \frac{€}{kg} \quad \text{(S6)}$$

- Sludge Retention Time affects management costs ($Cost_E$ and $Cost_{sludge}$) due to energy consumption (0.10-0.20 €/kWh) and sludge disposal (150 €/t of sludge, wet weight) by defining backwashing frequency, as treatment cycle duration (t_{cycle}, expressed in hours).

  Thus, treatment cycle duration can be derived from the definition of SRT, which is the ratio between the total amount of particulate matter in the reactor ($M_{TOT,r}$) and the amount of sludge removed per unit time. For submerged biofilters, sludge removal is achieved through backwashing; thus, sludge removal can be expressed as sludge removal for single backwashing ($\Delta M_{TOT,bw}$) divided by treatment cycle duration (t_{cycle}). Thus, SRT definition can be expressed by eq. S7 to eq. S9.

$$SRT[d] = \frac{M_{TOT,r}}{{}^{\Delta M_{TOT,bw}}/_{t_{cycle}}} \quad \text{(S7)}$$

$$M_{TOT,r} = \sum_{i=1}^{8} \left(X_{BH,i} + X_{P,i} + X_{S,i}\right) \cdot V_{cstr,i} \quad \text{(S8)}$$

$$\Delta M_{TOT,bw} = V_{bw} \cdot X_{TOT,bw} = (Q_{bw} \cdot t_{bw}) \cdot X_{TOT,bw} \quad \text{(S9)}$$

where $M_{TOT,r}$ is calculated in eq.S8 as the sum of particulate matter in each one of the eight reactors in series (with index *i* referring to the considered CSTR). At the same time, in eq. S9 $\Delta M_{TOT,bw}$ has been expressed following the backwashing procedure reported by Richard (1989) on real scale Biofor$^{(R)}$ for drinking water treatment plants. The volume of backwashing water (V_{bw}) has been determined considering a backwashing cycle duration (t_{bw}) of 1 h and a backwashing filtration rate 2 times the treatment cycle filtration rate, involving a total particulate matter concentration in backwashing water ($X_{TOT,bw}$) of 192 mg_{COD}/L. Thus, $\Delta M_{TOT,bw}$ can be expressed by eq. S10, where Q is the influent flow rate (in L/h), allowing the determination of t_{cycle} through eq. S11 and sludge disposal costs ($Cost_{sludge}$) through eq. S12.

$$\Delta M_{TOT,bw} = 2.1 \cdot Q \cdot 1\ h \cdot 192 \frac{mg_{COD}}{L} \quad \text{(S10)}$$

$$t_{cycle} = \frac{\Delta M_{TOT,bw}}{M_{TOT,r}} \cdot SRT \cdot 24\ {}^{h}/_{d} \quad \text{(S11)}$$

$$Cost_{sludge}\left[{}^{€}/_{yr}\right] = \Delta M_{TOT,bw} \cdot 10^{-6}\ {}^{kg_{COD}}/_{mg_{COD}} \cdot \frac{24\ {}^{h}/_{d} \cdot 365\ {}^{d}/_{yr}}{t_{cycle}} \cdot 0.15 \frac{€}{kg} \quad \text{(S12)}$$

The energy absorbed during a backwashing cycle has been then estimated considering the backwashing procedure normally recommended by biofilter's supplier (Degrémont S. A, 2010) and installed power for a pilot plant treating 0.6 m^3/h as 0.122 kWh per backwashing cycle and has been used for $Cost_E$ calculation through equation eq. S13.

$$Cost_E\left[{}^{€}/_{yr}\right] = \frac{365 \frac{d}{yr} \cdot 24 \frac{h}{d}}{t_{cycle}} \cdot\ 0.122\ kWh \cdot 0.15 \frac{€}{kWh} \quad \text{(S13)}$$

Investments and management cost contributions were grouped in a single cost function, considering an amortisation time of 10 years, through equations eq. S14.

$$OBJ_2 = Costs[€] = C_{invest} + 10yr \cdot \left(Cost_{reag} + Cost_E + Cost_{sludge}\right) \quad \text{(S14)}$$

As for the constraint functions of the model, the first constraint was set in order to limit biomass accumulation in the system at reasonable values considering the attachment capacity of the filter media. The maximum amount of particulate matter that can accumulate in the biofilter is equal to the volume of voids. Considering a biofilter filled with Biolite^{TM} with average diameter 3.5 mm and density 1.6 kg/m^3 (Degrémont S. A, 2010), a porosity (*e*) of 0.36 can be assumed [Aesoy et al., 1998]. Considering a particulate matter density (ρ_x) of 25 kg_{COD}/m^3 (Henze et al., 2008), the maximum particulate matter concentration has been calculated through equation eq. S15. This has led to the definition of the first constraint as expressed by eq. S17, which limits total particulate matter concentration under the value corresponding to 75% of reactor voids filled by particulate matter.

$$\frac{V_L \cdot e \cdot \rho_x}{V_L} = e \cdot \rho_x = 0.36 \cdot 25 \frac{kg_{COD}}{m^3} \cdot 10^3 = 9000 \frac{mg_{COD}}{L} \quad \text{(S15)}$$

$$CONSTR_1: (\overline{X_{TOT}}) \leq 0.75 \cdot 9000 \ \frac{mg_{COD}}{L} \quad \text{(S16)}$$

$$CONSTR_1: (\overline{X_{TOT}}) \leq 6750 \ \frac{mg_{COD}}{L} \quad \text{(S17)}$$

Then, the second constraint has been set to comply with the regulation limit for nitrate concentration in water treated for drinking purposes that is set at 50 $mgNO_3/L$, corresponding to 11.3 $mg_{NO3\text{-}N}/L$. In particular, it limits nitric nitrogen concentration in the biofilter effluent under the value corresponding to 75% of the regulation limit:

$$CONSTR_2: S_{NO3} \leq 0.75 \cdot 11.3 \frac{mg_N}{L} \quad \text{(S18)}$$

$$CONSTR_2: S_{NO3} \leq 8.5 \frac{mg_N}{L} \quad \text{(S19)}$$

Text S5. User interface of IND-NIMBUS

Interactive multiobjective optimization has been performed with IND-NIMBUS (Miettinen, 2006; Ojalehto et al., 2014), a software for nonlinear multiobjective optimization. An example screenshot of the graphical user-interface of IND-NIMBUS is reported in Figure S3

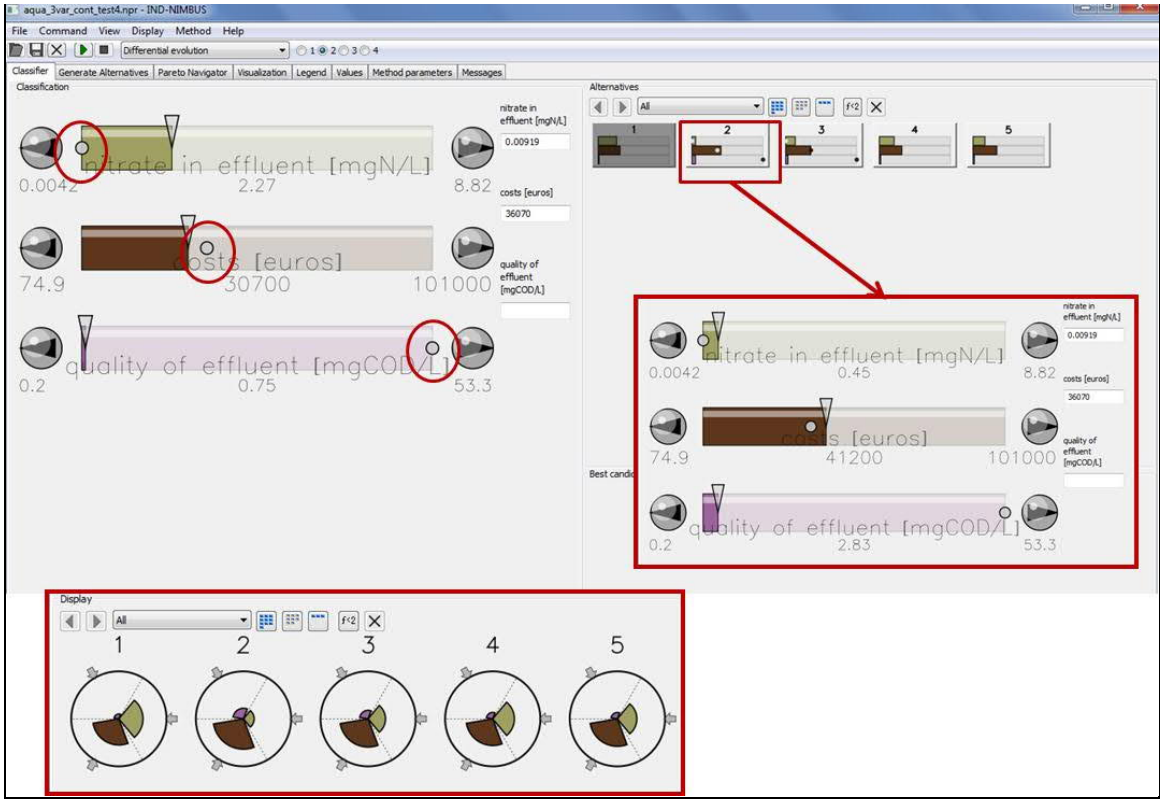

Figure S3 Screenshot of the graphical user interface of the IND-NIMBUS software

Text S6. Simulation models considered in the sensitivity analysis

Biological and physical processes considered by the models proposed by Kornaros and Lyberatos (Kornaros and Lyberatos, 1998) and Magrì and Flotats (Magrí and Flotats, 2008) have been presented in Table S1, while

specific stoichiometric coefficients, process rates and parameters are presented in Table S4, Table S6, Table S5 and Table S7 for Kornaros and Lyberatos (Kornaros and Lyberatos, 1998) model and for the Magrì and Flotats (Magrí and Flotats, 2008) model.

Table S1 Process rates in $mg_{COD} \cdot L^{-1} \cdot d^{-1}$ as described in the model by Kornaros and Lyberatos (Kornaros and Lyberatos, 1998).

Name	Process	Expression
$\mathbf{r_1}$	Aerobic Growth	$\hat{\mu}_H \cdot \left(\frac{S_S}{S_S + k_s}\right) \cdot \left(\frac{S_O}{S_O + k_{O,H}}\right) \cdot X_{BH} \cdot \vartheta^{T-20}$
$\mathbf{r_2}$	Anoxic growth on nitrate	$\eta_{g1} \cdot \hat{\mu}_H \cdot \left(\frac{S_S}{S_S + k_S}\right) \cdot \left(\frac{S_{NO3}}{S_{NO3} + k_{NO3}}\right) \cdot \left(\frac{k_O}{k_O + S_O}\right) \cdot X_{BH} \cdot \vartheta^{T-20}$
$\mathbf{r_3}$	Anoxic growth on nitrite	$\eta_{g2} \cdot \hat{\mu}_H \cdot \left(\frac{S_S}{S_S + k_S}\right) \cdot \left(\frac{S_{NO2}}{S_{NO2} + k_{NO2}}\right) \cdot \left(\frac{k_O}{k_O + S_O}\right) \cdot \left(\frac{k_{I,NO3}}{k_{I,NO3} + S_{NO3}}\right) \cdot X_{BH} \cdot \vartheta^{T-20}$
$\mathbf{r_4}$	Biomass decay	$b_H \cdot X_{BH} \cdot \vartheta^{T-20}$
$\mathbf{r_5}$	Hydrolysis of entrapped organics	$k_h \cdot \frac{X_S}{K_X \cdot X_{BH} + X_S} \cdot \left[\left(\frac{S_O}{S_O + k_{O,H}}\right) + \eta_h \cdot \left(\frac{k_{O,H}}{S_O + k_{O,H}}\right) \cdot \left(\frac{S_{NO3} + S_{NO2}}{S_{NO3} + S_{NO2} + k_{NO}}\right)\right] \cdot X_{BH}$

Table S2 Process rates in $mg_{COD} \cdot L^{-1} \cdot d^{-1}$ as described I the model by Magrì and Flotats (Magrí and Flotats, 2008).

Name	Process	Expression
$\mathbf{r_1}$	Aerobic Growth	$\hat{\mu}_H \cdot \left(\frac{S_S}{S_S + k_s}\right) \cdot \left(\frac{S_O}{S_O + k_{O,H}}\right) \cdot X_{BH} \cdot \vartheta^{T-20}$
$\mathbf{r_2}$	Anoxic growth on nitrate	$\eta_{g1} \cdot \hat{\mu}_H \cdot \left(\frac{S_S}{S_S + k_S}\right) \cdot \left(\frac{S_{NO3}}{S_{NO3} + k_{NO3}}\right) \cdot \left(\frac{k_O}{k_O + S_O}\right) \cdot X_{BH} \cdot \vartheta^{T-20}$
$\mathbf{r_3}$	Anoxic growth on nitrite	$\eta_{g2} \cdot \hat{\mu}_H \cdot \left(\frac{S_S}{S_S + k_S}\right) \cdot \left(\frac{S_{NO2}}{S_{NO2} + k_{NO2}}\right) \cdot \left(\frac{k_O}{k_O + S_O}\right) \cdot X_{BH} \cdot \vartheta^{T-20}$
$\mathbf{r_4}$	Biomass decay	$b_H \cdot X_{BH} \cdot \vartheta^{T-20}$
$\mathbf{r_5}$	Hydrolysis of entrapped organics	$k_h \cdot \frac{X_S}{K_X \cdot X_{BH} + X_S} \cdot \left[\left(\frac{S_O}{S_O + k_{O,H}}\right) + \eta_h \cdot \left(\frac{k_{O,H}}{S_O + k_{O,H}}\right) \cdot \left(\frac{S_{NO3} + S_{NO2}}{S_{NO3} + S_{NO2} + k_{NO}}\right)\right] \cdot X_{BH}$

Table S3 Model parameters and assumed values for the model by Kornaros and Lyberatos (Kornaros and Lyberatos, 1998).

Parameter	Value	Unit	Meaning
$\widehat{\boldsymbol{\mu}}_{\boldsymbol{H}}$	6	1/d	Maximum specific growth rate for heterotrophic biomass

$\mathbf{b_H}$	0.62	1/d	Decay rate for heterotrophic biomass
$\mathbf{k_h}$	3.0	1/d	Maximum specific hydrolysis rate
$\boldsymbol{\theta}$	1.03	-	Correction factor for temperature effect on biomass growth and decay rates
$\boldsymbol{\eta_{g1}}$	0.345	-	Correction factor for μ_h for anoxic growth on nitrate-nitrogen
$\boldsymbol{\eta_{g2}}$	0.411	-	Correction factor for μ_h for anoxic growth on nitrite-nitrogen
$\boldsymbol{\eta_h}$	0.4	-	Correction factor for hydrolysis under anoxic conditions
$\mathbf{k_s}$	20	mg_{COD}/L	Half-saturation constant for organic substrate
$\mathbf{k_{O,H}}$	0.2	mg_{COD}/L	Half-saturation constant for oxygen
$\mathbf{k_{NO3}}$	0.77	mg_N/L	Half-saturation constant for nitrate nitrogen
$\mathbf{k_{NO2}}$	0.28	mg_N/L	Half-saturation constant for nitrite nitrogen
$\mathbf{k_X}$	0.03	-	Half-saturation constant for slowly biodegradable substrate
$\mathbf{k_{I,NO3}}$	8.75	mg_N/L	Nitrate inhibition constant
$\mathbf{Y_h}$	0.46	mg_{COD}/mg_{COD}	Heterotrophic biomass yield, considering NO_3-N uptake for protein synthesis
$\mathbf{f_p}$	0.08	-	Fraction of biomass leading to particulate products
$\mathbf{i_{XB}}$	0.086	mg_N/mg_{COD}	Mass of nitrogen per mass of COD in biomass

169

170 **Table S4** Model parameters values assumed following the model presented by Magrì and Flotats (Magrí and
171 Flotats, 2008).

Parameter	Value	Unit	Meaning
$\boldsymbol{\hat{\mu}_H}$	4.16	1/d	Maximum specific growth rate for heterotrophic biomass
$\mathbf{b_H}$	0.17	1/d	Decay rate for heterotrophic biomass
$\mathbf{k_h}$	3.0	1/d	Maximum specific hydrolysis rate
$\boldsymbol{\theta}$	1.03	-	Correction factor for temperature effect on biomass growth and decay rates
$\boldsymbol{\eta_{g1}}$	0.23	-	Correction factor for μ_h for anoxic growth on nitrate-nitrogen
$\boldsymbol{\eta_{g2}}$	0.62	-	Correction factor for μ_h for anoxic growth on nitrite-nitrogen
$\boldsymbol{\eta_h}$	0.4	-	Correction factor for hydrolysis under anoxic conditions
$\mathbf{k_s}$	4	mg_{COD}/L	Half-saturation constant for organic substrate
$\mathbf{k_{O,H}}$	0.1	mg_{COD}/L	Half-saturation constant for oxygen
$\mathbf{k_{NO3}}$	0.5	mg_N/L	Half-saturation constant for nitrate nitrogen
$\mathbf{k_{NO2}}$	0.12	mg_N/L	Half-saturation constant for nitrite nitrogen
$\mathbf{k_X}$	0.03	-	Half-saturation constant for slowly biodegradable substrate

$\mathbf{Y_h}$	0.65	mg_{COD}/mg_{COD}	Heterotrophic biomass yield, considering NO_3-N uptake for protein synthesis
$\mathbf{f_p}$	0.08	-	Fraction of biomass leading to particulate products
$\mathbf{i_{XB}}$	0.086	mg_N/mg_{COD}	Mass of nitrogen per mass of COD in biomass

Text S7. Investigation of the feasible region

For the analysis of the feasible region (Section 2.4), 3000 random points were generated and corresponding constraint and objective function values were evaluated. The performed simulations showed that 41% of the points generated were feasible with respect to the constraints defined in Section 2.3. Constraint 1, on the total particulate matter concentration, turned out to be the main reason of infeasibility, as it was violated by 96% of the infeasible points. By plotting the generated random points in the design space (Figure S4a), it is possible to notice that points violating the first constraint are spread in the whole design space, and:

- in 61% of cases they are related to reactor volumes up to 600 L (the lower half of DV_1 range), while only 39% of points belong to the upper half of the DV_1 range (600 - 1200 L);
- in 58% of cases they correspond to a carbon dosage between 2 and 4 times the stoichiometric dosage (with only 42% occurring in case of Cdos lower than 2 times the stoichiometric dosage);
- in 69% of cases they are related to SRT higher than 50 d (upper half of DV_3 range) with only 31% occurring in case of SRT lower than 50 d.

These observations highlight the fact that, in a biodenitrification reactor, high values of total particulate matter concentration can be reached through different operating conditions, mainly related to low values of reactor volume, or high values of dosed carbon (non-limiting carbon substrate conditions) and high values of SRT (good biomass retention in the system). Considering the second constraint (on nitric nitrogen concentration), it was violated on the average by 2.5% of points. When looking at Figure S4a, one can notice that these points correspond to the lowest carbon dosages (C_{dos} lower than 5 mg_{COD}/L), meaning a carbon supply under 9.6% of the stoichiometric needs (calculated to be 52 mg_{COD}/L considering data reported in Section 2.1). These results highlight that carbon dosages under the stoichiometric requirements can be acceptable as far as the partial removal efficiency assures an acceptable output concentration and as far as endogenous carbon can sustain metabolic reactions and thus biological degradation. Below a certain level, represented by the 9.6% of stoichiometric dosage, the endogenous carbon is not enough and $NO_{3,out}$ concentration is no more acceptable. Figure S4b reports the generated random points in the objective space, for values of COD in the effluent lower than 20 mg_{COD}/L, thus, zoomed on the more informative portion of the space. However, points related to values of COD_{out} higher than 20 mg_{COD}/L have the same trend. The lowest nitrate removal efficiencies correspond to infeasible points because of the violation of constraint 2, indicating a carbon dosage not sufficient for the respect of 75% of the regulation limit on nitrate concentration. Increasing nitrate removal efficiencies corresponds to increasing costs and COD concentrations in the treated water, both following an exponential increase as the nitrate removal efficiency exceeds 90%. In this region, points violating constraint 1 correspond to lower costs. In case of partial removal of nitrate, both costs and COD concentrations in the effluent present

low values and could represent acceptable trade-offs, even if COD concentrations in the effluent should be mainly due to nitrite leaks, involving the systematic application of specific oxidation post-treatments. In order to limit the post-treatments to be applied, a Pareto optimal design should be found in the portion of feasible region characterized by an almost complete nitrate removal but further analysis needs to be performed and optimization is needed for it.

(a) (b)

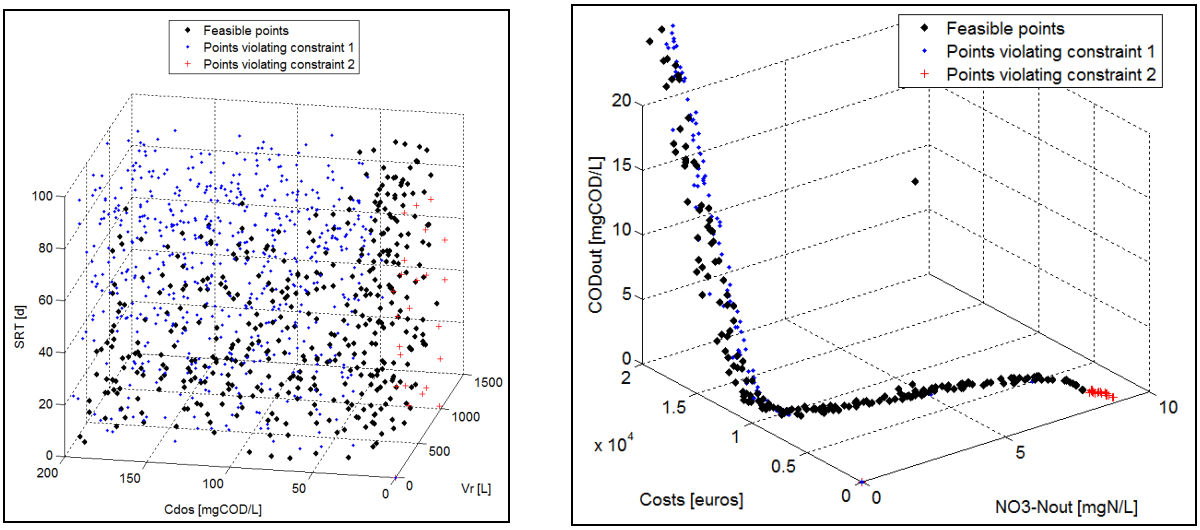

Figure S4. Feasible points (a) in the design space, and (b) their counterparts in the objective space (portion $COD_{out} \leq 20$ mg_{COD}/L).

More in details, Figure S5a represents generated feasible points in the design space with Figure S5b-d projecting them in 2D design space graphs. Figure S6a reports their representation in the objective space. Conflicts among objectives can be seen more clearly by plotting projections in 2D objective space graphs, as presented in Figure S6b-d. In particular, graphs in Figure S6b and Figure S6c show that points with lower values of objective 2 (Costs) and objective 3 (COD_{out}) involve the highest values of objective 1 (NO_3-N_{out}). On the contrary, Figure S6d shows that points with lower values of objective 2 (Costs) are also characterized by lower values of objective 3 (COD_{out}). From these observations, it can be concluded that the second and the third objective are not in conflict within each other, being on the other hand, both in conflict with the first objective.

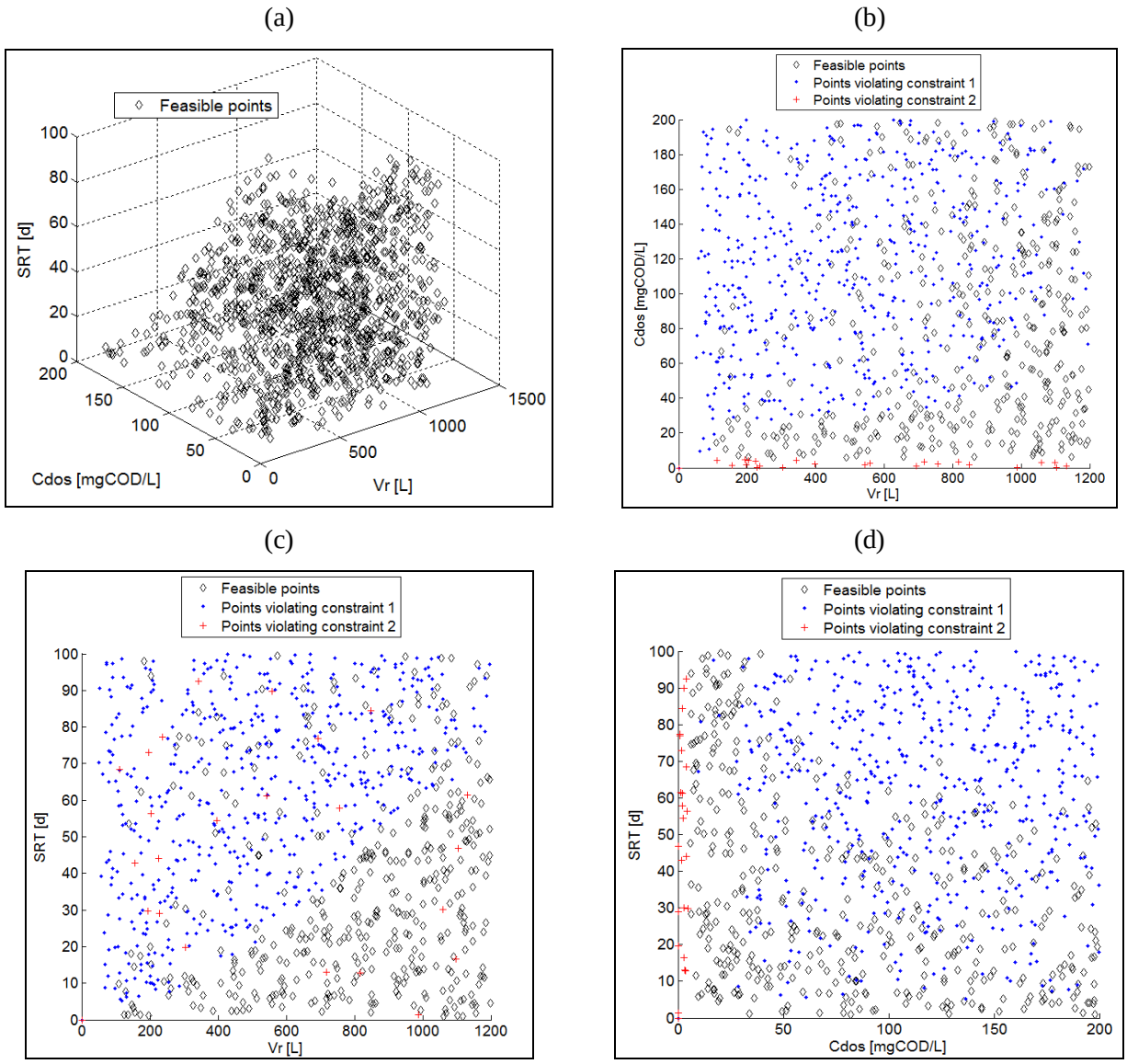

Figure S5. Representation of the results of the analysis of the feasible region in the design space: (a) Feasible points in the 3D plot; (b) Projection of feasible points in the 2D space (b) DV_2 as ordinate and DV_1 as abscissa; (c) DV_3 as ordinate and DV_1 as abscissa; (d) DV_3 as ordinate and DV_2 as abscissa.

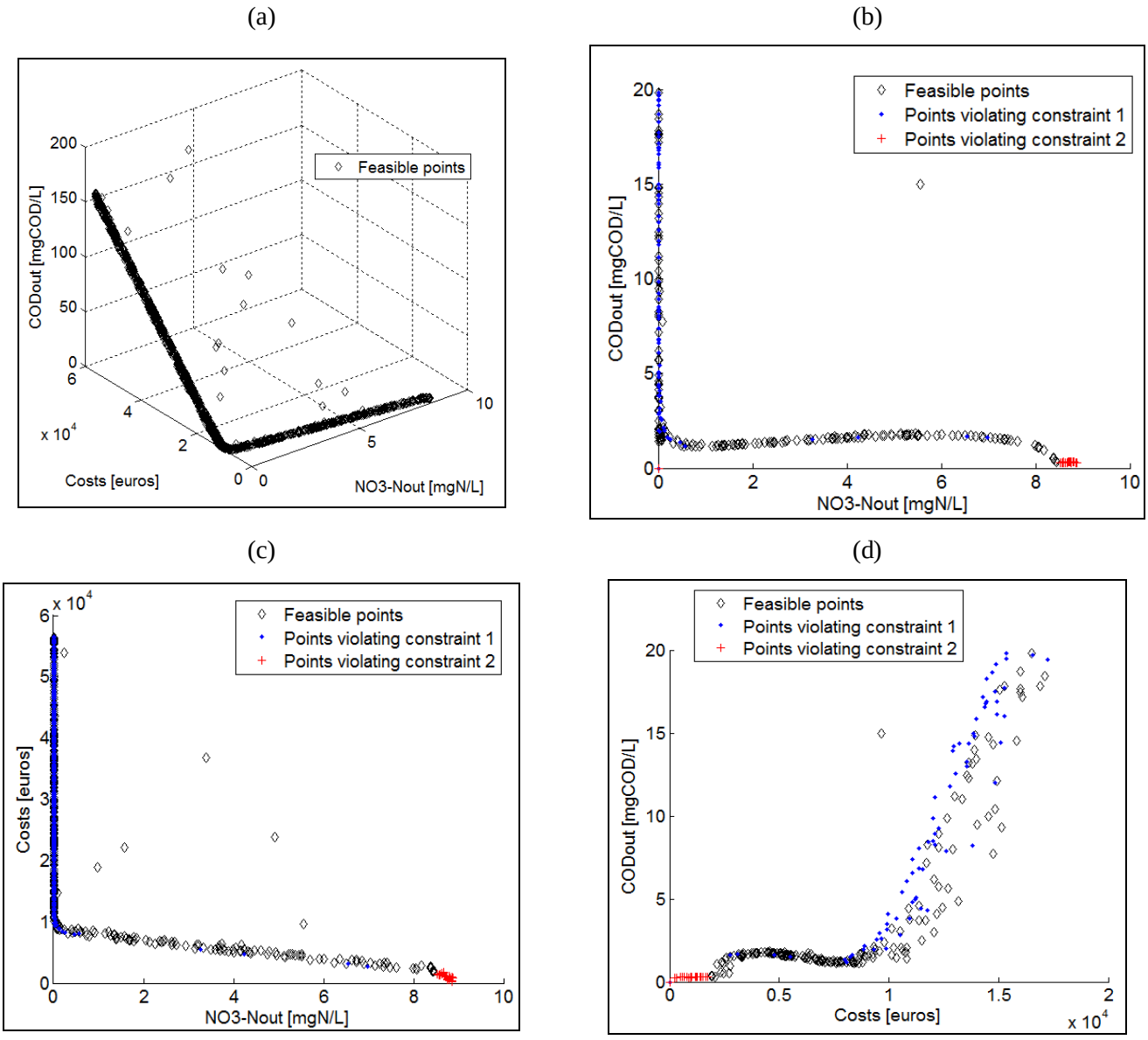

230 **Figure S6.** Projection of feasible points in the objectives space: (a) Feasible points in the 3D plot. Projection of
231 feasible points in the 2D space (b) OBJ_2 as ordinate and OBJ_1 as abscissa; (c) OBJ_3 as ordinate and OBJ_1 as
232 abscissa; (d) OBJ_3 as ordinate and OBJ_2 as abscissa.
233
234 **Text S8. Sensitivity analysis**
235 A sensitivity analysis has been performed varying few case-study specific parameters and the simulation model
236 as presented in Section 2.6. The variation of feasible points and constraint violations, with respect to the case
237 study results, is presented as bar charts in Figure S7.
238 As far as NGPM results are concerned, non-dominated solutions are represented in the design and objectives
239 spaces with case study results: Figure S2 reports results obtained when varying NO_3-N_{in} concentration and
240 influent flow rate, while Figure S3 reports results obtained when varying the concentration of biomass in
241 backwashing water, the number of CSTRs in series considered in the biofilter hydraulic model and the
242 simulation model. The distribution of obtained non-dominated solutions are compared in the box plot reported

in Figure S4, while the variation of mean and standard deviation with respect to the case study results presented in the manuscript, is presented in Figure S5.

As far as IND-NIMBUS results are concerned, the sensitivity analysis has been conducted performing five optimization steps that replicates considerations that guided the DM's choices in the case study:

1. problem initialization;
2. optimization looking for a similar value of OBJ_1, the best value for OBJ_3 and letting OBJ_2 change freely;
3. from the solution with lower OBJ_1 value, optimization looking for the best OBJ_1 value, letting both OBJ_2 and OBJ_3 change freely;
4. optimization to an acceptable level of OBJ_2 and OBJ_3 letting OBJ_1 change freely;
5. optimization to an acceptable level of OBJ_1, OBJ_2 and OBJ_3;
6. identification of the most preferred design among proposed Pareto optimal solutions (i.e. designs)

Pareto optimal solutions obtained through the sensitivity analysis are reported in Figure S6 and Figure S7. Then, Figure SI.8 reports the variation of most preferred designs compared to the case study one, detailing the evaluation for each design variable and objective function.

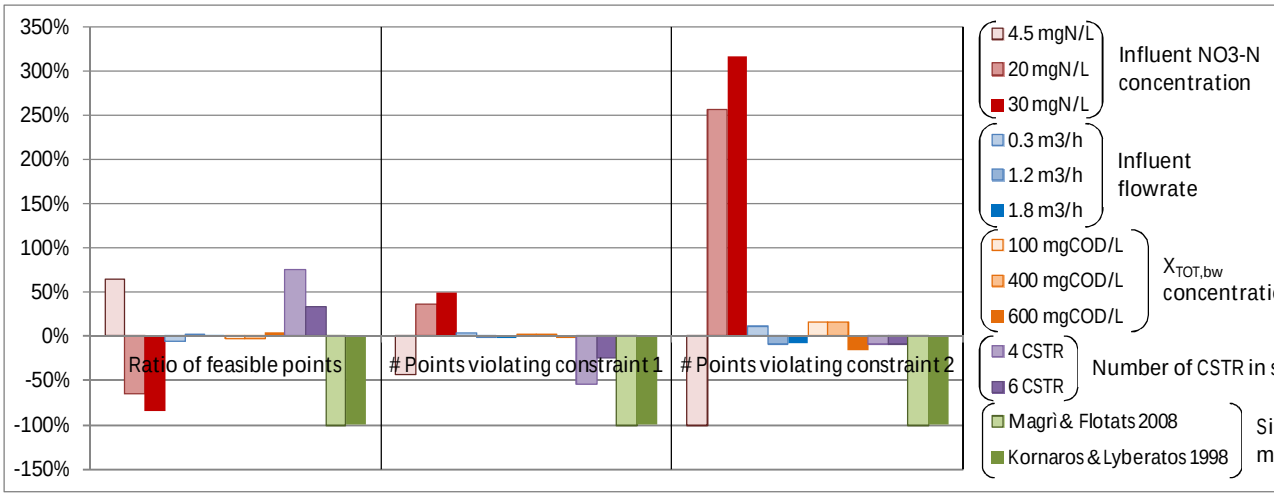

Figure S1. Sensitivity analysis on feasible region results: variations observed on feasible point ratio and on the number of points violating each constraint.

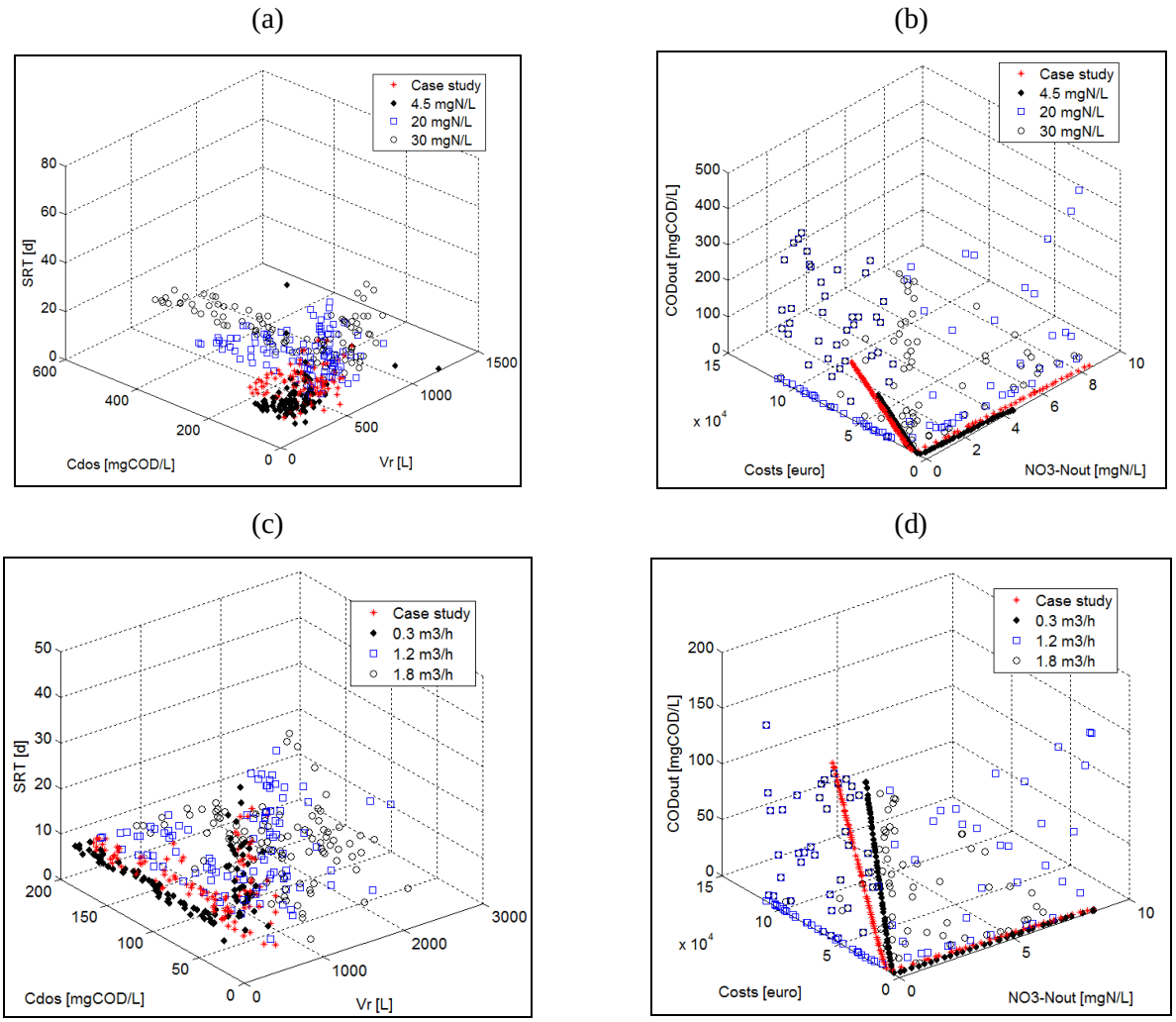

Figure S2. NGPM results obtained varying nitric nitrogen concentration in raw water and influent flowrate represented with case study results respectively in the design (a, c) and the objectives spaces (b, d).

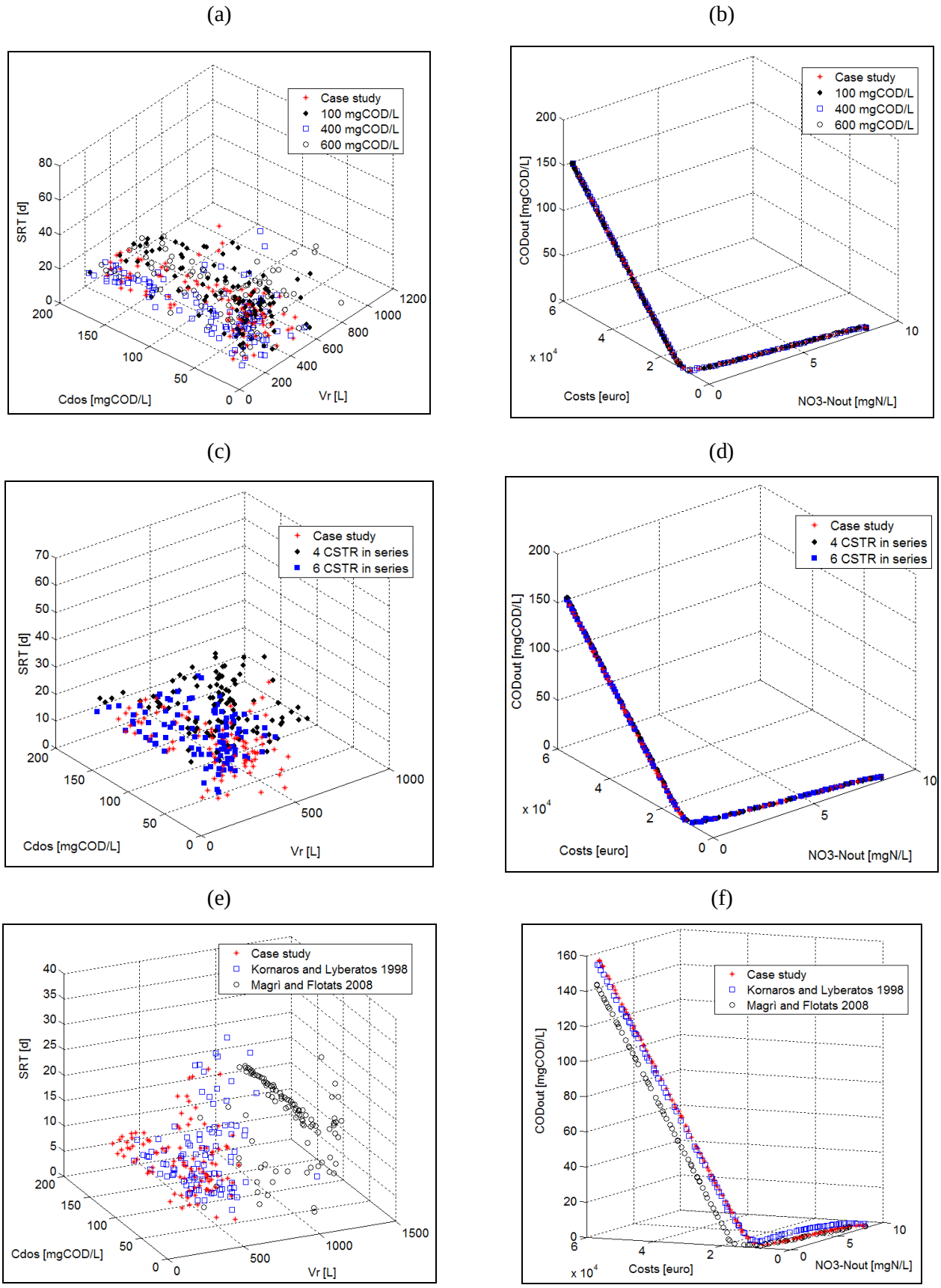

Figure S3. NGPM results obtained varying the concentration of biomass in backwashing water, the number of CSTRs in series considered in the biofilter hydraulic model and the simulation model represented with case study results respectively in the design (a, c, e) and the objectives spaces (b, d, f).

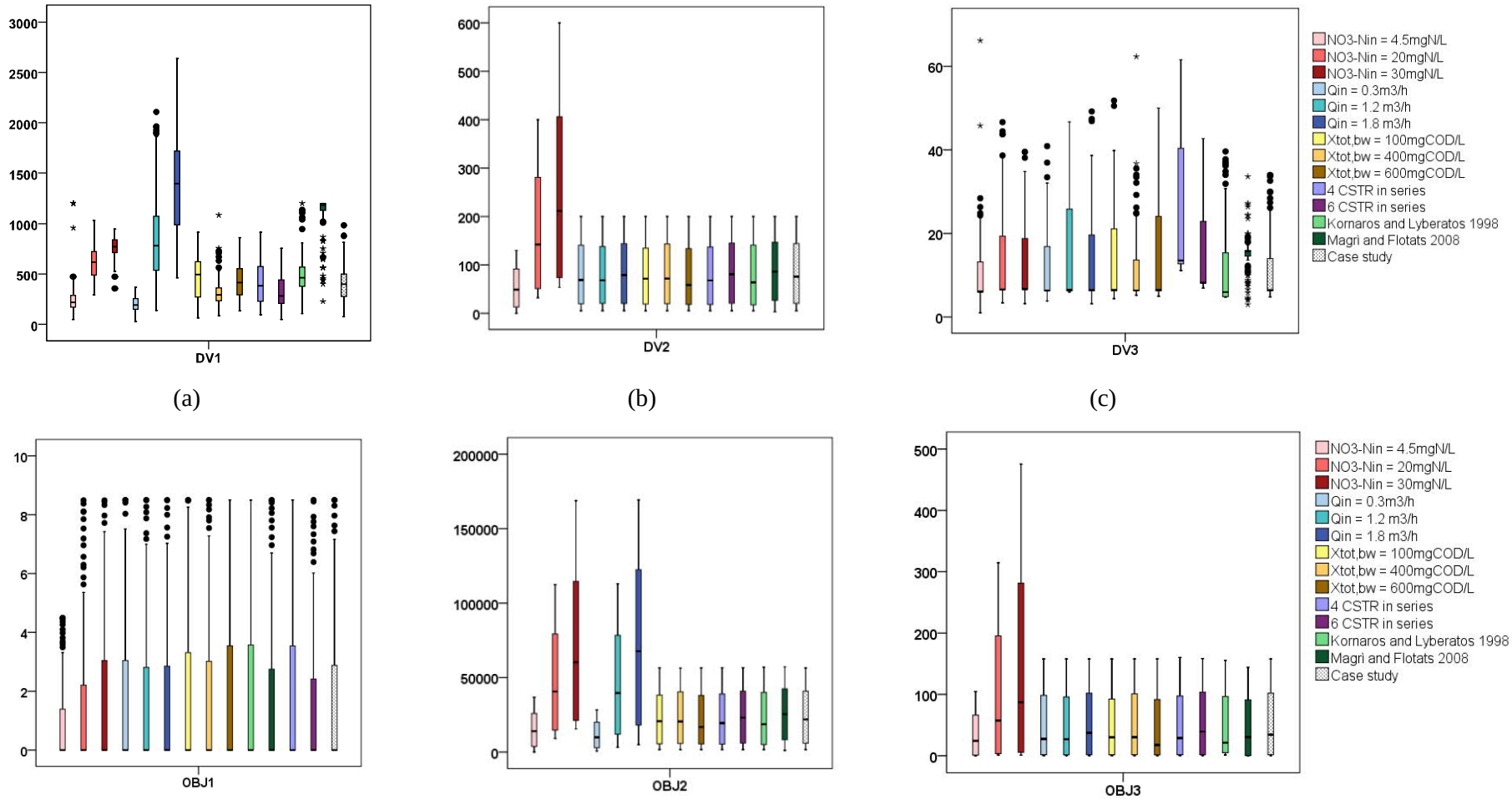

(a) (b) (c)

(b) (c) (d)

Figure S4. Distributions of NGPM results for different values of selected case specific parameters and for different simulation models, compared to case study results. Values for (a) design variable 1, (b) design variable 2, (c) design variable 3, (d) objective function 1, (e) objective function 2, (f) objective function 3.

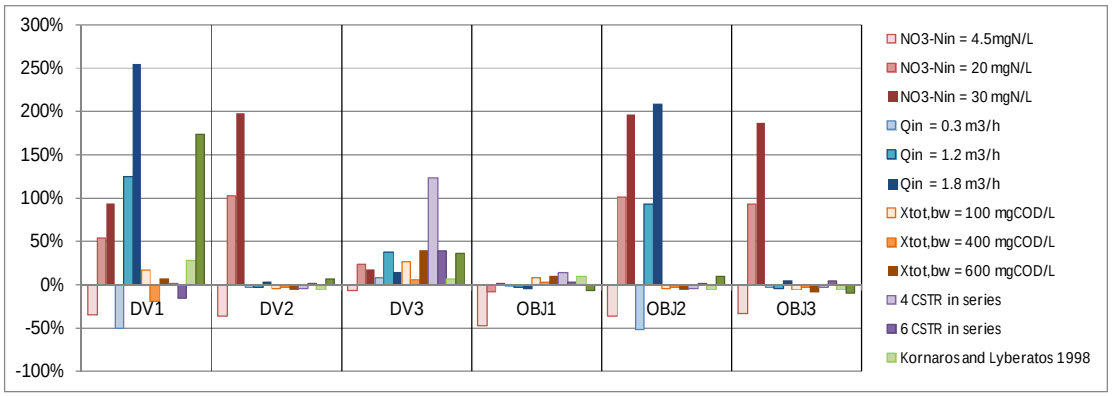

(a)

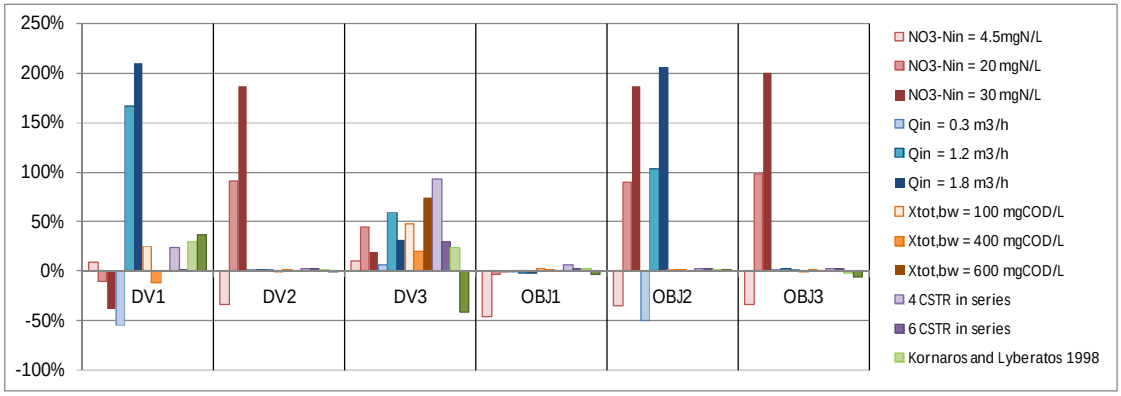

(b)

Figure S5. Variation of mean (a) and standard deviation (b) values for design variables and objective functions of NGPM results obtained through sensitivity analysis.

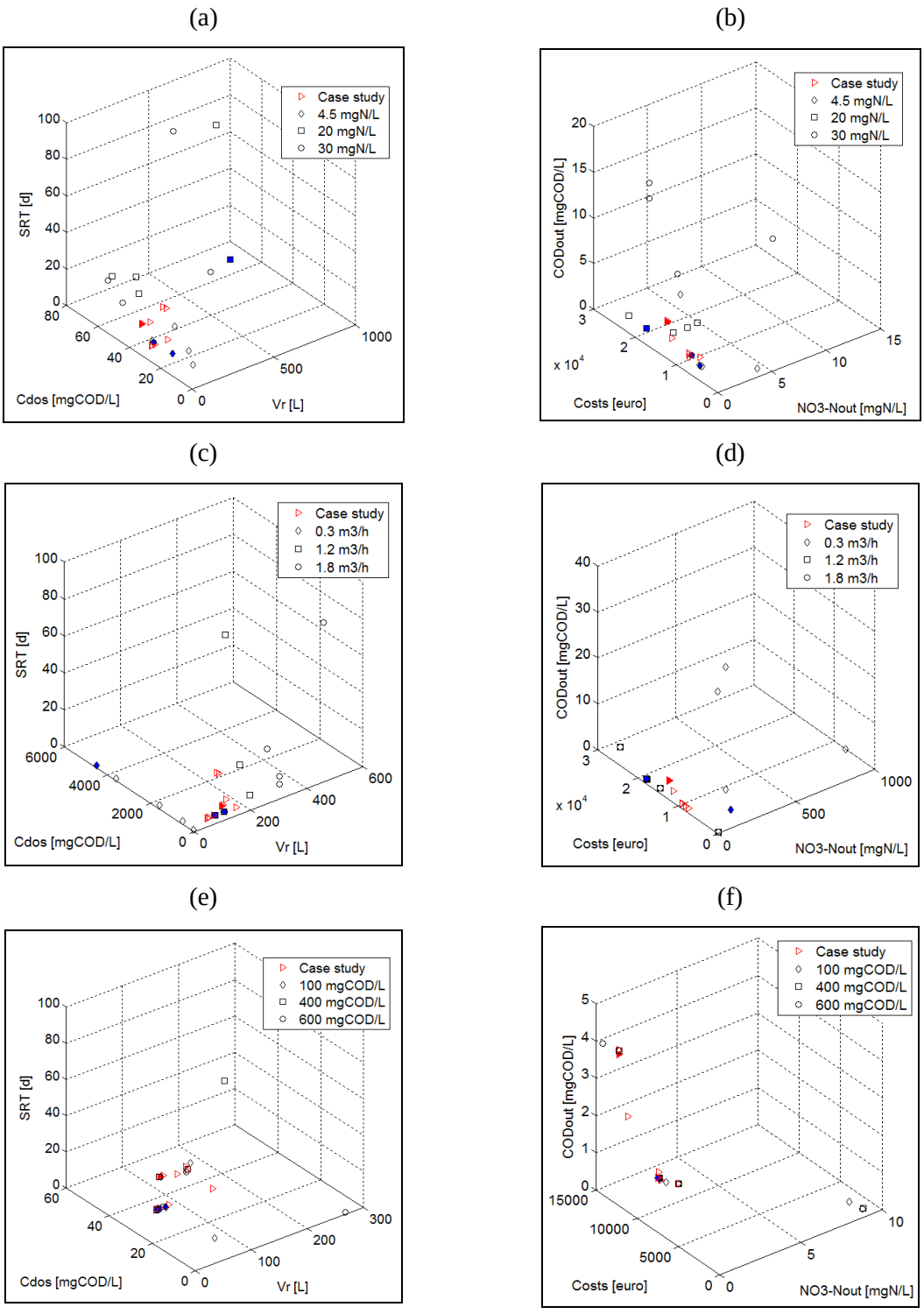

Figure S6. Pareto optimal solutions generated by IND-NIMBUS by varying nitric nitrogen concentration in raw water (a,b), influent flow rate (c,d) and concentration of biomass in backwashing water (e,f). Solutions represented with case study results in the design (a, c, e) and the objectives spaces (b, d, f). Most preferred solutions have been represented as filled points.

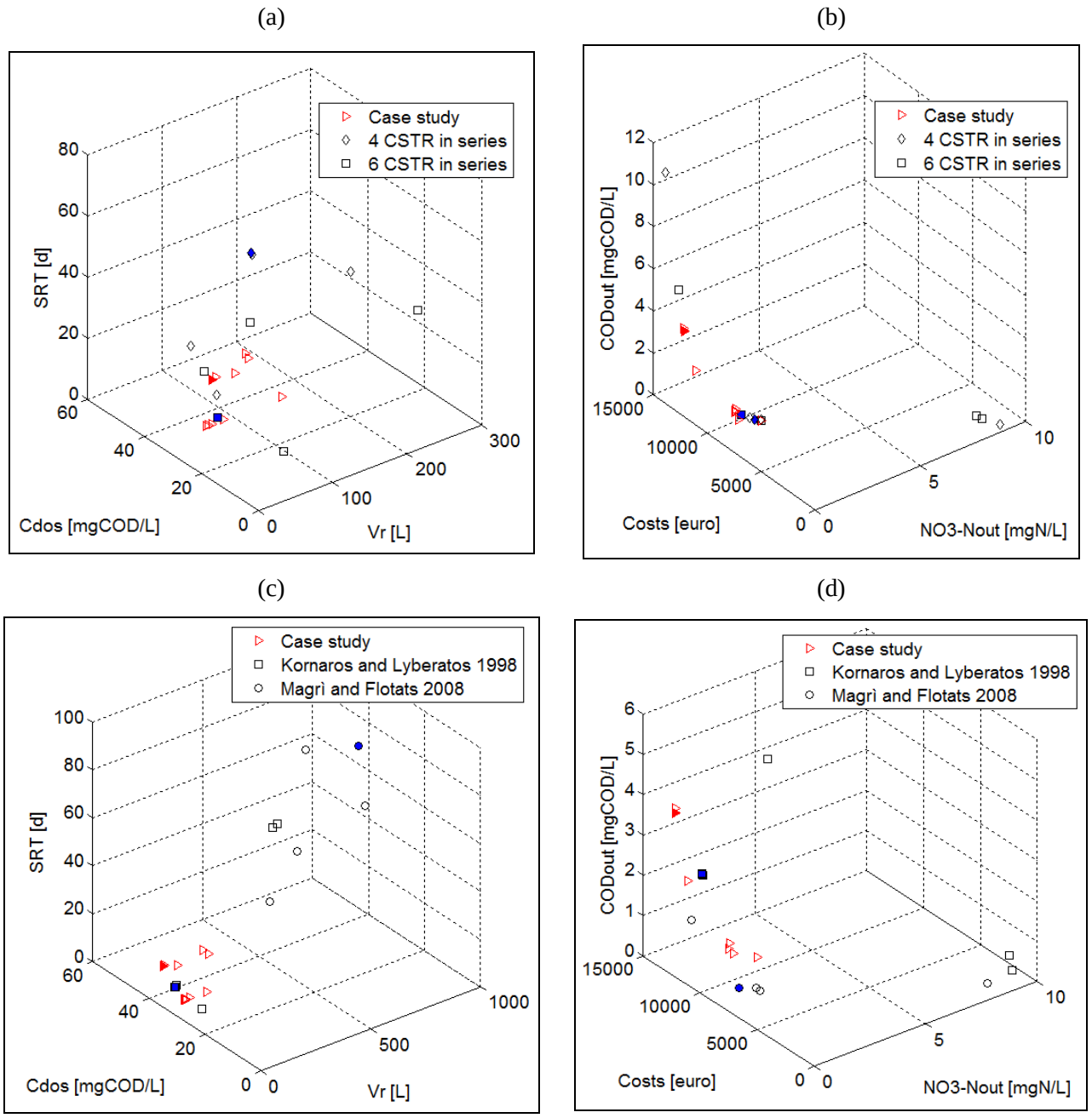

Figure S7. Pareto optimal solutions generated by IND-NIMBUS by varying the number of CSTRs considered in the biofilter hydraulic model (a,b) and the simulation model (c,d): solutions represented with case study results in the design (a, c) and objectives spaces (b, d). Most preferred solutions have been represented as filled points.

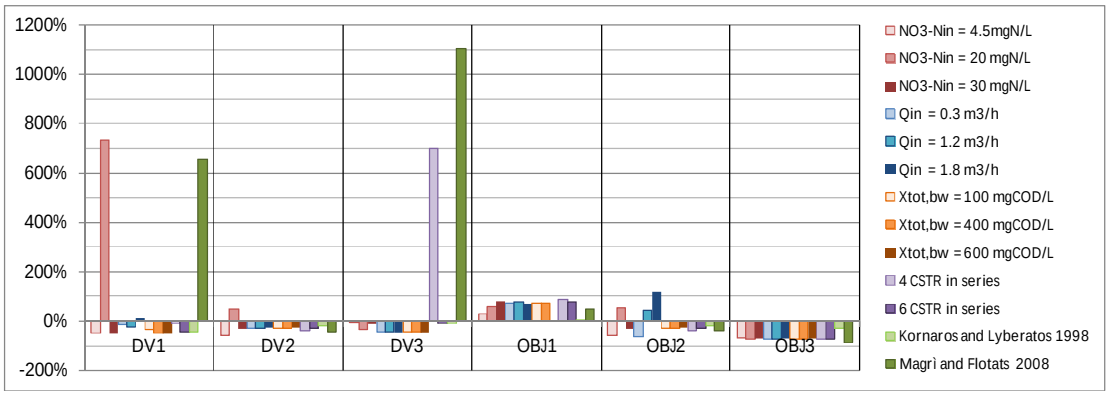

Figure SI.8. Variation of design variables and objective functions values of most preferred design found through IND-NIMBUS sensitivity analysis.

References

Boltz, J.P., Morgenroth, E., Sen, D., 2010. Mathematical modelling of biofilms and biofilm reactors for engineering design. Water Sci. Technol. 62, 1821–1836. doi:10.2166/wst.2010.076

Degrémont S. A, 2010. Water treatment handbook. Ondeo - Degrémont.

Henze, M., Gujer, W., Mino, T., van Loosdrecht, M.C.M., Task Group on Mathematical Modelling for Design and Operation of Biological Wastewater Treatment., 2000. Activated sludge models ASM1, ASM2, ASM2d and ASM3. IWA Publishing.

Henze, M., van Loosdrecht, M., Ekama, G., Brdjanovic, D., 2008. Biological wastewater treatment : principles, modelling and design. IWA Publishing.

Her, J.-J., Huang, J.-S., 1995. Influences of carbon source and C/N ratio on nitrate/nitrite denitrification and carbon breakthrough. Bioresour. Technol. 54, 45–51. doi:10.1016/0960-8524(95)00113-1

Huang, J.-S., Her, J.-J., Jih, C.-G., 1998. Kinetics of denitritification and denitratification in anoxic filters. Biotechnol. Bioeng. 59, 52–61. doi:10.1002/(SICI)1097-0290(19980705)59:1<52::AID-BIT7>3.0.CO;2-S

Kornaros, M., Lyberatos, G., 1998. Kinetic modelling of pseudomonas denitrificans growth and denitrification under aerobic, anoxic and transient operating conditions. Water Res. 32, 1912–1922. doi:10.1016/S0043-1354(97)00403-X

Lazarova, V., Capdeville, B., Nikolov, L., 1994. Influence of seeding conditions on nitrite accumulation in a denitrifying fluidized bed reactor. Water Res. 28, 1189–1197. doi:10.1016/0043-1354(94)90207-0

Lazarova, V.Z., Capdeville, B., Nikolov, L., 1992. Biofilm Performance of a Fluidized Bed Biofilm Reactor for Drinking Water Denitrification. Water Sci. Technol. 26, 555–566. doi:10.2166/wst.1992.0435

Magrí, A., Flotats, X., 2008. Modelling of biological nitrogen removal from the liquid fraction of pig slurry in a sequencing batch reactor. doi:10.1016/j.biosystemseng.2008.08.003

Miettinen, K., 2006. IND-NIMBUS for Demanding Interactive Multiobjective Optimization, in: Multiple Criteria Decision Making ’05. The Karol Adamiecki University of Economics in Katowice, Katowicei, pp. 137–150.

Morgenroth, E., van Loosdrecht, M.C.M., Wanner, O., 2000. Biofilm models for the practitioner. Water Sci. Technol. 41, 509–512. doi:10.2166/wst.2000.0486

Nurizzo, C., Mezzanotte, V., 1992. Groundwater Biodenitrification on Sand Fixed Film Reactor Using Sugars as Organic Carbon Source. Water Sci. Technol. 26, 827–834. doi:10.2166/wst.1992.0463

Ojalehto, V., Miettinen, K., Laukkanen, T., 2014. Implementation aspects of interactive multiobjective optimization for modeling environments: the case of GAMS-NIMBUS. Comput. Optim. Appl. 58, 757–779. doi:10.1007/s10589-014-9639-y

Ordaz, A., Oliveira, C.S., Quijano, G., Ferreira, E.C., Alves, M., Thalasso, F., 2012. Kinetic and stoichiometric characterization of a fixed biofilm reactor by pulse respirometry. J. Biotechnol. 157, 173–179. doi:10.1016/j.jbiotec.2011.10.015

Plattes, M., Fiorelli, D., Gillé, S., Girard, C., Henry, E., Minette, F., O'Nagy, O., Schosseler, P.M., 2007. Modelling and dynamic simulation of a moving bed bioreactor using respirometry for the estimation of kinetic parameters. Biochem. Eng. J. 33, 253–259. doi:10.1016/j.bej.2006.11.006

Plattes, M., Henry, E., Schosseler, P.M., Weidenhaupt, A., 2006. Modelling and dynamic simulation of a moving bed bioreactor for the treatment of municipal wastewater. Biochem. Eng. J. 32, 61–68. doi:10.1016/j.bej.2006.07.009

Pujol, R., Hamon, M., Kandel, X., Lemmel, H., 1994. Biofilters: flexible, reliable biological reactors. Water Sci. Technol. 29, 33–38. doi:10.2166/wst.1994.0742

Richard, Y.R., 1989. Operating Experiences of Full-Scale Biological and Ion-Exchange Denitrification Plants in France. Water Environ. J. 3, 154–167. doi:10.1111/j.1747-6593.1989.tb01503.x

Tang, Y., Ziv-El, M., Zhou, C., Shin, J.H., Ahn, C.H., Meyer, K., McQuarrie, J., Candelaria, D., Swaim, P., Scott, R., Rittmann, B.E., 2011. Using carrier surface loading to design heterotrophic denitrification reactors. J. Am. Water Works Assoc. 103, 68–78. doi:10.1002/j.1551-8833.2011.tb11421.x

Tchobanoglous, G., Stensel, H.D., Tsuchihashi, R., Franklin, B., Abu-Orf, M., Bowden, G., Pfrang, W., 2014. Wastewater Engineering: Treatment and Resource Recovery, Fifth. ed. Metcalf and Eddy, Inc., McGraw-Hill Book Company, New York, U.S.A.

Vrtovšek, J., Roš, M., 2006. Denitrification of Groundwater in the Biofilm Reactor with a Specific Biomass Support Material, Acta Chimica Slovenica .